J. of Thermal Science Vol.10, No.1

Numerical Investigation of Developing Turbulent Flow in a Helical Square Duct with Large Curvature

Gao Hui Guo Liejin

State Key Laboratory of Multiphase Flow in Power Engineering, Xi'an Jiaotong University, Xi'an 710049, China

A fully elliptic numerical study has been carried out to investigate the three-dimensional turbulent developing flow in a helical square duct with large curvature. A two-layer zonal model is proposed and used, in which the whole region is divided into a viscosity-affected near wall layer and a fully turbulent region. A DSM closure is applied in the former, and a one-equation model is solved in the latter. The results presented in this paper cover a Reynolds number range of $(1\sim10)\times10^4$. The development of flow is found to be dominated by radial pressure gradient and Dean-type secondary motion. The distribution of Reynolds stresses in fully developed flow exhibit a complex pattern of turbulence anisotropy. The development of peripherally averaged friction factor and the distribution of local friction factor in fully developed flow are given and discussed.

Keywords: curved pipe, developing flow, turbulence model, numerical simulation.

Introduction

Curved pipes, such as bends, helical coils, spiral coils etc., are extensively used in piping systems. Although a large amount of work have been published regarding pressure loss, heat transfer and detailed flow mechanisms of curved pipe flow[1,2], more experimental and numerical study are still deserved, especially for the case of developing flow, turbulent flow and non-circular cross section.

Numerical simulation of turbulent curved pipe flow is a challenging task for its inherent features, including complex secondary flow, turbulence anisotropy and significant elliptical effects in the case of mild and high curvature. The earliest work on the problem was done by Patankar et al.[3], who solved the parabolic Navier-Stokes equation for developing flow using k-ε model. However, the parabolic equations are only applicable for pipes with a very small curvature[1,2] . Li et al.[4] and Lin et al.[5] carried out a fully elliptic numerical study of developing turbulent flow and heat transfer in helical pipe using renormalized group (RNG) k-ε model and standard k-ε model respectively. To mimic the anisotropic turbulence behavior, Iacovides et al. proposed a reflection-free differential second moment (DSM) model[6] and several versions of algebraic second-moment (ASM) model[7] when they made simulation of turbulent flow and heat transfer in square-sectioned U-bends. Their results show advantages of adopting a Reynolds-stress closure rather than an eddy-viscosity model across the fully turbulent region, and also demonstrate that the wall function approach need to be replaced by a low Reynolds number model across the viscosity-affected region to predict the near-wall secondary flow with sufficient accuracy. Large-eddy simulation was also used in the computation of fully developed turbulent flow in a curved tube[8] and developing flow in a U-bend with square cross section[9].

The present study is devoted to the turbulent flow through a square-sectional helical pipe. Experimental friction factors and Nusselt numbers were reported by Butuzov et al.[10] and Kadambi[11]. Little work has concerned with the detailed flow mechanisms of this situation. By solving a set of fully elliptic equations with a two-layer zonal turbulence model, this paper attempts to discover the procedure of flow development and the characteristics of the fully developed flow. The physics considered here is characterized by Reynolds number $Re = (1\sim10)\times10^4$, that is, the Dean number $De = (0.407 \sim 4.07)\times10^4$.

Received 2000

Nomenclature

			physical basis (m/s)
C_1, C_2	modeling coefficients	x',y'	local coordinates (m)
De	Dean number		**Greeks**
D_H	hydraulic diameter (m)	δ_{ij}	Kroncker delta
k	turbulent kinetic energy (m^2/s^2)	ε	dissipation rate of turbulent kinetic energy (m^2/s^3)
P	generation rate of turbulence (m^2/s^3)	θ	longitudinal angle from curved section entry (°)
Re	Reynolds number	μ	dynamic viscosity ($kg\cdot m^2/s$)
Re_s	wall-distance-based turbulent Reynolds number	ρ	density (kg/m^3)
R	radial distance to the helical axis (m)	σ_k	modeling constant
s	the distance from wall to cell center (m)	υ	kinematic viscosity (m^2/s)
U	time-averaged velocity (m/s)	ϕ	redistribution rate of turbulence (m^2/s^3)
W	time-averaged streamwise velocity (m/s)		**Subscripts**
W_b	bulk velocity (m/s)	i, j, k	general spatial indices
u, v, w	fluctuating velocity components in the orthogonal	in, out	inner, outer

Physical Model and Numerical Details

Pipe configuration and system of coordinates

Flow geometry and system of coordinates are shown in Fig.1. The helical square duct, with a 260 mm curved diameter, 93 mm pitch, and a 43×43 mm cross-section area, is preceded and followed by a section of straight duct. The computation is performed in the Cartesian coordinates, while an orthogonal physical basis, viz. the tangent, the normal, and the binormal of the centerline of the duct, is adopted for flow field visualization. Both velocity and Reynolds stress tensor are transformed and exhibited on the physical basis. A local two-dimensional coordinate system (x', y') is established for each cross section with coordinate axis pointing to the inverse direction of the normal and binormal vector respectively.

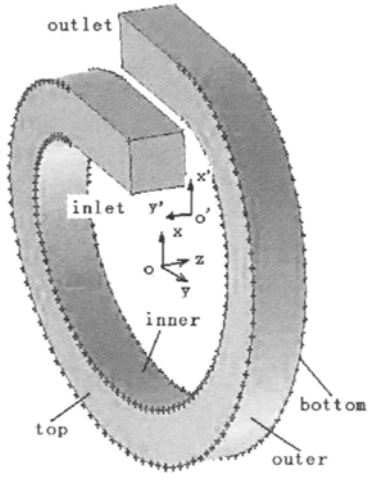

Fig.1 Flow geometry and coordinate system

Governing equations and boundary conditions

The three-dimensional fully elliptic Reynolds equations[6] and continuity equation describing the incompressible turbulent flow are solved in this paper. Nonslip boundary condition is imposed on the pipe wall. Uniform distribution of velocity and turbulent variables are assumed at the inlet. The turbulent variables could be computed from an estimated turbulence intensity (5%) and a turbulent length scale ($0.07D_H$)[4]. At the outlet, an uniform value was set to the static pressure of the fluid, while all other conditions are extrapolated from the interior of the domain.

Turbulence model

In the two-layer zonal turbulence model, the whole region is divided into a fully turbulent region and a viscosity-affected layer based on a wall-distance-based turbulent Reynolds number, Re_s, defined as

$$\mathrm{Re}_s \equiv \frac{\rho\sqrt{k}s}{\mu} \tag{1}$$

In the former (Re_s > 200), a high-Re DSM closure is applied, while in the latter (Re_s < 200), a low-Re one-equation model[12] is employed.

The DSM involves calculation of the unknown Reynolds stresses using differential transport equations:

$$U_k\frac{\partial}{\partial x_k}(\overline{u_iu_j}) = -\left(\overline{u_iu_k}\frac{\partial U_j}{\partial x_k} + \overline{u_ju_k}\frac{\partial U_i}{\partial x_k}\right) + \phi_{ij} - \varepsilon_{ij} + d_{ij} + \frac{\partial}{\partial x_k}\left(\nu\frac{\partial\overline{u_iu_j}}{\partial x_k}\right) \tag{2}$$

The symbols ϕ_{ij}, ε_{ij} and d_{ij} denote, respectively, the pressure-strain, dissipative, and turbulent diffusive processes, all of which require modeling. As usual, viscous dissipation is assumed to be isotropic:

$$\varepsilon_{ij} = \frac{2}{3}\delta_{ij}\varepsilon \tag{3}$$

Turbulent diffusion d_{ij} is simplified by using a scalar turbulent diffusivity as follows:

$$d_{ij}=\frac{\partial}{\partial x_k}\left(\frac{\mu_t}{\rho\sigma_k}\frac{\partial\overline{u_iu_j}}{\partial x_k}\right),\ \sigma_k=0.82 \qquad (4)$$

According to a modified linear pressure-strain model[13], Φ_{ij} is decomposed into a "slow pressure-strain" term and a "rapid pressure-strain" term as follows:

$$\phi_{ij}=-C_1\frac{\varepsilon}{k}\left(\overline{u_i'u_j'}-\frac{2}{3}\delta_{ij}k\right)-C_2\left(P_{ij}-\frac{2}{3}\delta_{ij}P_{kk}\right) \qquad (5)$$

where, P_{ij}, the stress production, is the first term of the right hand side of equation (2), and the values of C_1 and C_2 are functions of the Reynolds stress invariants and the turbulent Reynolds number. The "wall-reflection" term included in classical approach is omitted following the suggestion given by Iacovides et al.[6,7].

Numerical Aspects

The computation is based on the SIMPLEC algorithm. Second-order upstream scheme is used in the discretization of differential equations. A nonuniform grid of 45 × 45 is used to map the cross section of the duct, while 120 intervals (90 in the curved section) are used in the axial direction. Grid independence test shows that, with finer grid, there are only slight differences between the predicted mean velocities and turbulent stresses. The algebraic equations are solved by algebraic multigrid algorithm (AMG).

Results and Discussion

Validation

Due to the limited experimental data concerning the helical square duct turbulent flow in the literature, we considered the developing flow in a square-sectioned U-bend[14] with a radius of curvature equal to $3.37D_H$, at $Re = 5.67\times10^4$, as a test case of our turbulence model and numerical scheme. A comparison between the computed results and experimental measurements[14] along the plane located halfway between the wall and the symmetry plane is shown in Fig.2 . In addition to the two-layer model, the k-ε model and a DSM incorporated with wall function are evaluated. In point of fact, there is only small difference of the streamwise velocity prediction between the two models incorporated with wall functions, while the two-layer model shows a better capture of the minimum that appears in the 90° and 130° sections. The corresponding shear stress profiles exhibit more pronounced differences, and generally, the two-layer model achieves somewhat closer agreement with experiment.

Development of Flow Field

The development of flow field is exposed with

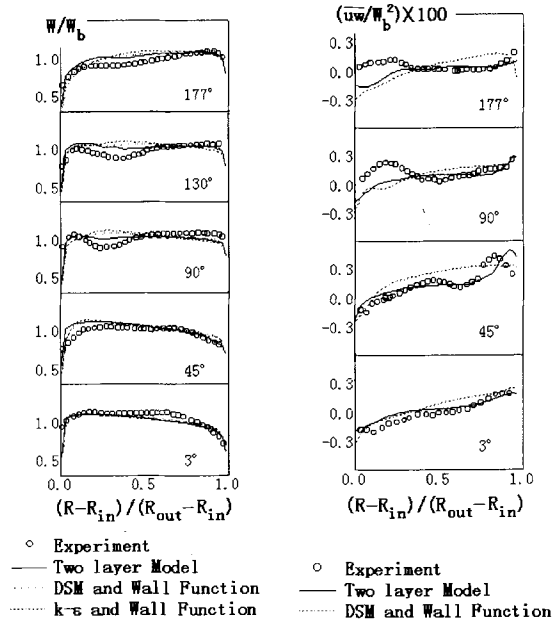

(a) streamwise velocity (b) turbulent shear stress

Fig.2 Comparisons between measured and computed profiles of velocity and turbulent shear stress, for flow in a square-sectioned U-bend[14], at Re = 5.67×10^4

contour plots of streamwise velocity and vector plots of secondary flow in cross-sectional planes at various angle in Fig.3 for the flow at $Re = 5.67\times10^4$.

In general, radial pressure gradient (from the outer wall to the inner wall) and Dean-type secondary flow, ascribing to the inherent centrifugal effect[1,2], are two key factors affecting the flow development. As radial pressure gradient is formed immediately at the inlet of the curved section and disappears as soon as the fluid leaves it, nonuniform streamwise pressure gradients are prevail at both the entry and the exit. At the entry, there is a strong flow acceleration along the inner wall in accordance with the favorable longitudinal pressure gradient there. While, at the exit, the fluid near the outer wall is accelerated for the same reason. With the flow development from the curved section entry, the axial pressure gradient become uniform, and at the same time the Dean-type secondary motion causes a substantial deformation of the streamwise velocity contours by forcing the low-speed fluid inward near the wall and the high-speed fluid outward in the central part of the cross-section. As a result, high-speed flow is increasingly displaced towards the outer wall and the side wall, whereas fluid with low velocity accumulates at the inner wall. Within the domain of axial angle $210°<\theta<320°$, the axial flow shows little change, indicating a fully developed situation.

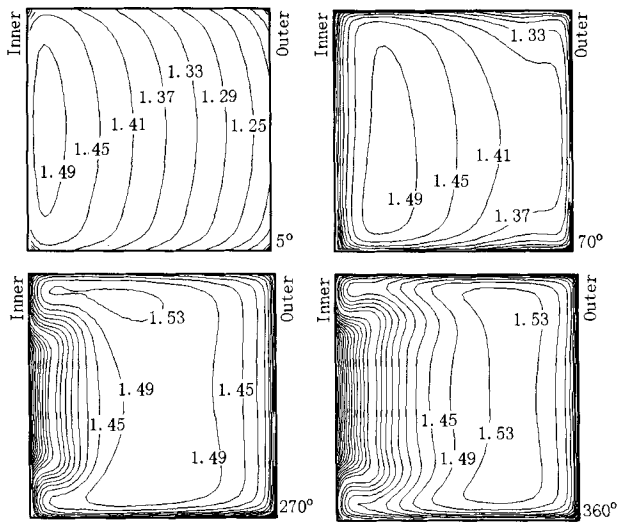

(a) Contours of nondimensional streamwise velocity, W/W_b

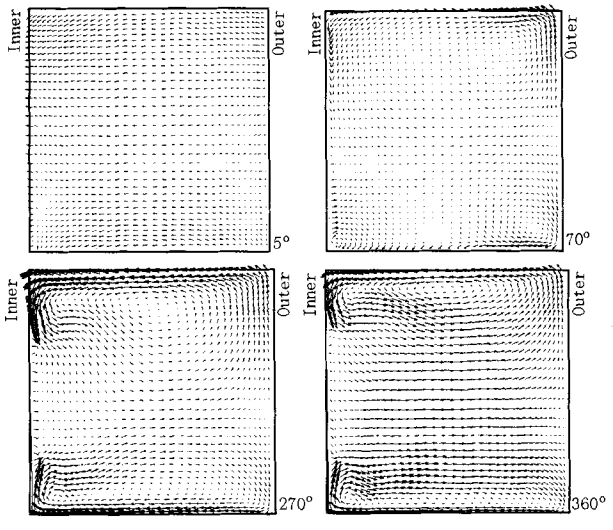

(b) Vector plots of secondary flow

Fig.3 Development of flow field at $Re = 5.67 \times 10^4$

The vector plots show a inward motion at the entry of the curved section, associated primarily with the inviscid coupling of the mean velocity and pressure fields. After $\theta = 30°$, the Dean-type secondary flow is formed and augmented in a wavily pattern, until the fully developed situation is reached. At the outlet, large secondary flow is enlarged further, and it is also associated with the inviscid coupling. The pressure-driven secondary flow takes the form of two counter-rotating vortices with a forward stagnation region at the center of the outer wall. Large secondary flows present along the sidewall and part of the inner wall. There is one or two small vortices embedded in the two large ones near the inner corner.

The asymmetry of the velocity field indicates that the finite pitch has a substantial effect on the helical duct flow. The upper vortex of the secondary flow is enlarged while the lower one is depressed. By the axial angle $\theta = 90°$, the axial flow is shifted to the lower half of the cross-section, and then it is shifted to the upper half until the developed situation is reached. In the vicinity of the 360° plane, the flow recovers its symmetry to some extent.

Reynolds Stresses of the Fully Developed Flow

The components of Reynolds stress tensor (normalized by W_b^2) for the fully developed flow at $Re = 5.67 \times 10^4$ are presented in contoured form in Fig.4. The stresses show high values near the walls, where shearing is greatest, diminishing towards the core of the flow. Stabilizing effect due to convex curvature at the inner wall is responsible for lowering the turbulence intensity there whereas destabilizing concave curvature effect at the outer wall raises it. The secondary motion counteract the stabilizing and destabilizing effects of these walls. Along the side walls, the high turbulence-energy fluid is driven from the outer wall to the inner. In turn, stabilized flow with

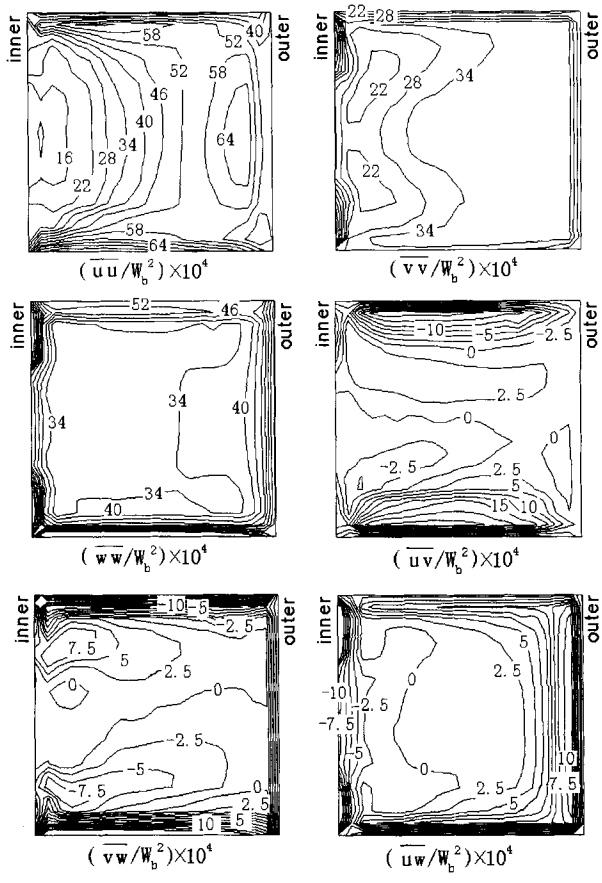

Fig.4 Contours of turbulent stresses for $\theta = 270°$ at $Re = 5.67 \times 10^4$

low turbulence energy at the inner wall is convected along the symmetry plane into the core region. In addition to wall curvature and secondary motion, pressure strain, turbulent diffusion and dissipation, all affect the distribution of the stresses, which results in a complex pattern of turbulence anisotropy. In general, the normal stresses are larger than the shear ones, while each of them exhibits different distribution from one another.

Friction Factor

The peripherally averaged friction factors in the curved section is shown in Fig.5. The curves for all situations show sharp decrease initially. Then the variation are slowed down and eventually the curves become quite flat, indicating the situation of fully developed flow. The friction factor shows prominent oscillation at $Re = 1 \times 10^4$. However, this behavior becomes weak at high Reynolds number. It also could been seen that the flow developed more rapidly at higher Reynolds number. The numerical predictions of the friction factor for fully developed flow ($Re = 2 \times 10^4$, 5.67×10^4 and 10×10^4) are about 10~20% lower than that computed from the experimental correlations[10][15]. As the correlations are derived from experiments of turbulent flow through slightly or mildly curved pipe with negligible pitch, this discrepancy could be ascribed to the effect of finite pitch and large curvature of the helical duct considered here. Further investigations on this subject are demanded.

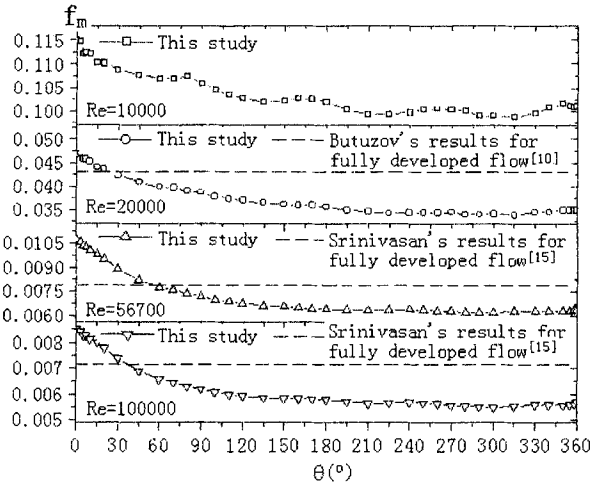

Fig.5 The development of peripherally averaged friction factor with axial position at various *Re*

Fig.6 shows the peripheral distribution of local friction factor in the case of the fully developed flow. The data are plotted in the direction from bottom to top along the inner and outer walls, or from inner to outer along the side walls. The friction factors at the side walls exhibit similar distribution with higher values present near the inner wall, while in general the values at the top wall are substantially larger than those at the bottom wall. The curves for the inner wall and the outer wall are close to symmetric. There are two peaks near the two ends and a step in the middle of the curve for the inner wall. The curve for the outer wall are quite flat except for sharp variations near the two ends. This pattern of the local friction factor distribution is in accordance with the mean velocity field depicted previously.

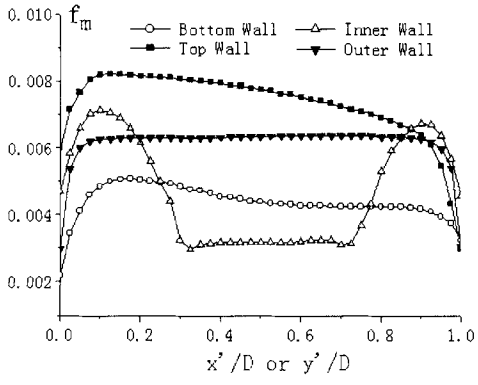

Fig.6 Distribution of local friction factor for $\theta = 270°$ at $Re = 5.67 \times 10^4$

Conclusions

From the analysis in this paper, it can be concluded that:

1. The two-layer zonal model used in this paper is superior in predicting the developing turbulent flow through a square sectioned U-bend[14] in comparison with the k-ε model and DSM with wall function, especially for the Reynolds stress field. Thus, it is indirectly verified that this model is qualified to predict the same kind of flow considered here.

2. The flow development is found to be dominated by radial pressure gradient and Dean-type secondary flow. Fully developed flow is formed within the domain of axial angle $210° < \theta < 320°$. The flow field is distorted as a consequence of finite pitch.

3. As a consequence of wall curvature ,secondary motion and other factors such as pressure strain, turbulent diffusion and dissipation, the Reynolds stresses exhibit a complex pattern of anisotropy.

4. The peripherally averaged friction factor decreases as the flow developing until the fully developed situation is reached. The predicted results of fully developed flow are lower than those calculated

from the experimental correlations derived from the case of small/mild curvature and negligible pitch. The peripheral distribution of local friction factor in the case of fully developed flow is also depicted.

References

[1] Ito, H.. Flow in Curved Pipes", JSME Int. J., 1987, 30: (262): 543-551

[2] Berger, S.A., Talbot, L, Yao, L.S.. Flow in Curved Pipes. Ann. Rev. Fluid Mech., 1983, 15: 461-513

[3] Patankar, S.V., Pratab, V.S., Spalding, D.B.. Prediction of Turbulent Flow in Curved Pipes. J. Fluid Mech., 1974, 67: 583-595

[4] Li, L.J., Lin, C.X., Ebadian, M.A.. Turbulent Mixed Convective Heat Transfer in the Entrance Region of a Curved Pipe with Uniform Wall Temperature. Int. J. Heat Mass Transfer, 1998, 41(23): 3793-3805

[5] Lin, C.X., Ebadian, M.A.. Developing Turbulent Convective Heat Transfer in Helical Pipes. Int. J. Heat Mass Transfer, 1997, 40(16): 3861-3873

[6] Iacovides, H., Launder, B., Li, H.Y.. Application of a Reflection-free DSM to Turbulent Flow and Heat Transfer in a Square-sectioned U-bend. Int J. Heat and Fluid Flow, 1996, 17: 22-33

[7] Iacovides, H., Launder, B., Li, H.Y.. The Computation of Flow Development through Stationary and Rotating U-ducts of Strong Curvature. Int J. Heat and Fluid Flow, 1996, 17: 22-33

[8] Boersma, B.J., Nieuwstadt, F.T.M.. Large-eddy Simulation of Turbulent Flow in a Curved Pipe. ASME J. Fluids Eng., 1996, 118: 248-254

[9] Zeng, S., Manners, A.. Large-eddy Simulation of Turbulent Flow in a Square Duct with 180° Bend. (In Chinese), J. Tsinghua Univ. (Sci. & Tech.), 1999, 39(4): 100-103

[10] Butuzov, A.I., Bezrodnyy, M.K., Pustovit, M.M.. Hydraulic Resistance and Heat Transfer in Forced Flow in Rectangular Coiled Tubes. Heat Transfer-Sov. Res., 1975, 7(4): 84-88

[11] Kadambi, V.. Heat Transfer and Pressure Drop in a Helically Coiled Rectangular Duct. ASME Paper, No.83-WA/HT-1, 1983

[12] Chen, H.C., Patel, V.C.. Near-wall Turbulence Models for Complex Flows including Separation. AIAA Journal, 1988, 26(6): 641-648

[13] Launder, B.E., Shima, N.. Second-Moment Closure for the Near-Wall Sublayer: Development and Application. AIAA Journal, 1989, 27(10): 1319-1325

[14] Chang, S.M., Humphrey, J.A.C.H., Modavi, A.. Turbulent Flow in a Strongly Curved U-Bend and Downstream Tangent of Square Cross Section. Phys. Chem. Hydrodyn., 1983, 4: 243-269

[15] Srinivasan, P.S., Nandapurkar, S.S., Holland, F.A.. Friction Factors for Coils. Trans. Inst. Chem. Eng., 1970, 48: 156-161